



Contents lists available at ScienceDirect

## Deep-Sea Research I

journal homepage: [www.elsevier.com/locate/dsr](http://www.elsevier.com/locate/dsr)

# The effects of random surface waves on the steady Ekman current solutions <sup>☆</sup>

Jin-Bao Song <sup>a,b,\*</sup><sup>a</sup> Institute of Oceanology, Chinese Academy of Sciences, Nanhai Road 7, Qingdao 266071, PR China<sup>b</sup> Key Laboratory of Ocean Circulation and Waves (KLOCAW), Chinese Academy of Sciences, Qingdao 266071, PR China

## ARTICLE INFO

*Article history:*

Received 29 April 2008

Received in revised form

8 December 2008

Accepted 21 December 2008

Available online 1 January 2009

*Keywords:*

Ekman current

Random wave

Stokes drift

Eddy viscosity coefficient

## ABSTRACT

The response of near-surface current profiles to wind and random surface waves are studied based on the approach of Jenkins [1989. The use of a wave prediction model for driving a near surface current model. *Dtsch. Hydrogr. Z.* 42, 134–149] and Tang et al. [2007. Observation and modeling of surface currents on the Grand Banks: a study of the wave effects on surface currents. *J. Geophys. Res.* 112, C10025, doi:10.1029/2006JC004028]. Analytic steady solutions are presented for wave-modified Ekman equations resulting from Stokes drift, wind input and wave dissipation for a depth-independent constant eddy viscosity coefficient and one that varies linearly with depth. The parameters involved in the solutions can be determined by the two-dimensional wavenumber spectrum of ocean waves, wind speed, the Coriolis parameter and the densities of air and water, and the solutions reduce to those of Lewis and Belcher [2004. Time-dependent, coupled, Ekman boundary layer solutions incorporating Stokes drift. *Dyn. Atmos. Oceans* 37, 313–351] when only the effects of Stokes drift are included. As illustrative examples, for a fully developed wind-generated sea with different wind speeds, wave-modified current profiles are calculated and compared with the classical Ekman theory and Lewis and Belcher's [2004. Time-dependent, coupled, Ekman boundary layer solutions incorporating Stokes drift. *Dyn. Atmos. Oceans* 37, 313–351] modification by using the Donelan and Pierson [1987. Radar scattering and equilibrium ranges in wind-generated waves with application to scatterometry. *J. Geophys. Res.* 92, 4971–5029] wavenumber spectrum, the WAM wave model formulation for wind input energy to waves, and wave energy dissipation converted to currents. Illustrative examples for a fully developed sea and the comparisons between observations and the theoretical predictions demonstrate that the effects of the random surface waves on the classical Ekman current are important, as they change qualitatively the nature of the Ekman layer. But the effects of the wind input and wave dissipation on surface current are small, relative to the impact of the Stokes drift.

© 2008 Elsevier Ltd. All rights reserved.

<sup>☆</sup> The research presented in this paper was supported by National Science Fund for Distinguished Young Scholars (no. 40425015), the High-Tech Research and Development Program of China (863 program, no. 2006AA09A309) and the Fund for Creative Research Groups by NSFC (no. 40821004).

\* Correspondence to: Institute of Oceanology, Chinese Academy of Sciences, Nanhai Road 7, Qingdao 266071, PR China.  
Tel.: +86 532 82898506; fax: +86 532 82898506.

E-mail address: [songjb@ms.qdio.ac.cn](mailto:songjb@ms.qdio.ac.cn)

## 1. Introduction

Ocean surface currents, waves, and related atmosphere–ocean boundary layer processes have received increasing attention by researchers and marine forecasters in recent years because of their importance to numerous and wide-ranging topics in environmental- and safety-related studies. For example, they are important for the interpretation of satellite images and the impacts of surface

currents on satellite-derived wind estimates (Quilfen et al., 2001; Kelly et al., 2001), the correction of biases in radar-derived surface currents (Chapron et al., 2005), sea ice drift (Tang and Gui, 1996), various biological processes such as the drift of fish eggs and larvae (Brickman and Frank, 2000; Reiss et al., 2000), environmental loading on offshore structures (Farmer et al., 1995), and the dispersion and drift of oil and other pollutants (Leibovich, 1997a,b; Morinta et al., 1997). Additional examples include weather, hurricane intensities (Emanuel, 1999; Andreas and Emanuel, 2001), and climate (Tang et al., 2002) because of their role in the transport of heat, moisture, and momentum.

Theoretical descriptions for the response of the near-surface current profile to pure wind forcing are well established, the details of the response depending principally upon the vertical variation of the eddy viscosity and density structure (e.g., see Ekman, 1905; Madsen, 1977). The classical Ekman theory (Ekman, 1905), assuming a balance between Coriolis force and the divergence of momentum transfer by turbulence stress, predicted a perfect current profile, the Ekman spiral. However, observational evidence does not directly support the classical Ekman model (Price and Sundermeyer, 1999; Lewis and Belcher, 2004; Polton et al., 2005). Measurements of the steady mean current suggest that the surface current lies at an angle of between  $10^\circ$  and  $45^\circ$  to the surface wind stress (Huang, 1979) except there exist the differences between the Lagrangian current measurements (which include the Stokes drift) and the quasi-Eulerian current discussed here, the current is deflected by approximately  $75^\circ$  from the wind stress at a depth between 5 and 20 m (Price and Sundermeyer, 1999) and rapidly attenuated below the surface. But the classical Ekman model predicts a surface deflection of exactly  $45^\circ$ , and the associated subsurface currents die off far too slowly to provide a realistic representation of the observed results (Lewis and Belcher, 2004).

Advances have been made recently in tackling the above-mentioned discrepancies between theory and observations. These studies show that the influence of the surface wave motion via the Stokes drift and mixing is fundamental to understanding the observed Ekman current profiles (Lewis and Belcher, 2004; Polton et al., 2005; Rasclé et al., 2006), although real Ekman currents are the products of a host of interrelated factors, including wind stress, surface wave motion, surface heating and so on. The Stokes drift can substantially affect the whole of the mixed layer in two ways, as Lewis and Belcher (2004) stated. First, it deforms the vorticity associated with the mixed layer turbulence generating Langmuir circulations. These streamwise vortices enhance the local turbulent kinetic energy and are believed to regulate the depth of the mixed layer. Second, it deforms the planetary vorticity via a modified Coriolis force term in the linear horizontal momentum equations, altering the balance of the mean flow in the mixed layer. Lewis and Belcher (2004), and also Polton et al. (2005), studied the impact of the Stokes–Coriolis term on the Eulerian Ekman spiral by incorporating this wave-induced Stokes–Coriolis forcing into the momentum balance of the Ekman layer, with an

unstratified water column. The analytical solution they presented is shown to agree reasonably well with current profiles from observations and certainly agrees much better than the classical Ekman model. They also reported that the Stokes drift is the key to reconciling the discrepancies in the angular deflections of the steady-state currents. Saetra and Albretsen (2007) also found that including the Stokes–Coriolis forcing increased the angular turning of the surface current. In fact, the Stokes drift has a vertical attenuation scale of  $1/(2k)$  (where  $k$  is the dominant wavenumber) with the magnitude can be as large as the classical Ekman current, it is approximately in the same direction as the wind direction, and the Stokes–Coriolis forcing perpendicular to wind direction, both the Stokes drift and the Stokes–Coriolis forcing will affect the angle between the wind and surface current. So, the Stokes drift has to be considered for discussing surface currents and their directions. However, the good agreement found by Lewis and Belcher (2004) and Polton et al. (2005) is not obtained with the model presented by Rasclé et al. (2006) for unstratified and Rasclé (2007) for stratified conditions. They argued that the stratification is an important factor to the large deflection angle and the surface trapping of the Ekman current as stated by Price and Sundermeyer (1999). The conclusions of these investigations on the importance of stratification appear to be compelling, and it seems that the effects of stratification need to be carefully considered. But, in this paper, we also ignore the effects of stratification to develop an analytical solution for a steady-state Ekman equation modified by the Stokes drift, wind input and wave dissipation, to display the effects of surface waves, over and beyond just including a Stokes drift term as studied by Lewis and Belcher (2004) and Polton et al. (2005), and to look at the impact of including reduced wind stress associated with wave generation and momentum transfer from waves to mean flow by wave dissipation.

In fact, the effect of the wind in producing currents in the ocean is complicated considerably by the presence of wind-generated surface waves as presented by Ursell (1950), Longuet-Higgins (1953, 1960), Hasselmann (1970), Pollard (1970), and Huang (1979). Waves grow and evolve in space and time, interacting with ocean currents and reflecting the structure and development of the wind stress fields that generate them. As they experience wave breaking and dissipation, momentum passes from waves into ocean currents. Using irrotational theory for wave growth and wave breaking, Weber (1983), Weber and Melsom (1993), and Melsom (1996) investigated the conversion of the wave pseudo-momentum to momentum of the mean Eulerian current from wave dissipation caused by the eddy viscosity. Jenkins (1986, 1987a,b, 1989) developed the corresponding formulation based on an ocean spectral wave model. Perrie et al. (2003) coupled the formulation of Jenkins (1987a,b, 1989) to a simple linear diagnostic ocean model with an Ekman layer and a depth-independent eddy viscosity to investigate the impact of waves on surface currents. They showed that the wave effect could increase the surface current by as much as 40%. Followed the methodology developed by

Perrie et al. (2003), Tang et al. (2007) used more advanced ocean and wave models to compute wind-driven currents and wave spectra in order to obtain an improved estimate of the wave effects on surface currents. In this paper, analytic steady solutions are presented for modified Ekman equations including random surface wave effects following the approach of Jenkins (1987a, b, 1989) and Perrie et al. (2003) when the eddy viscosity coefficient is, respectively, taken as depth independent and proportional to depth. The effects of random waves on the classical Ekman current are then studied by comparing the solutions including waves to those with no waves. We also compared the solutions with those presented by Lewis and Belcher (2004), who included only the effects of Stokes drift.

## 2. Basic equations and boundary conditions

In the absence of surface waves, the steady wind-driven Ekman horizontal currents satisfy the following standard Ekman equation for a deep, vertically homogeneous ocean, of infinite lateral extent

$$ifU_E = \frac{\partial}{\partial z} \left( A_v \frac{\partial U_E}{\partial z} \right), \quad (1)$$

where  $U_E(z) = u_E(z) + iv_E(z)$  is the complex horizontal velocity in the  $x$ - $y$  plane,  $i = \sqrt{-1}$ ,  $f$  is the Coriolis parameter, the horizontal coordinate axes are fixed on the still water level with  $z = 0$ , the  $z$ -axis is along the vertical direction with positive direction upwards,  $A_v = A_v(z)$  is the vertical eddy viscosity coefficient. The surface boundary condition for the Ekman current is

$$A_v \frac{\partial U_E}{\partial z} \Big|_{z=0} = \frac{\tau_a}{\rho_w}, \quad (2)$$

where  $\rho_w$  is the water density,  $\tau_a = \tau_{ax} + i\tau_{ay}$  is the complex wind stress, computed from surface wind fields  $\mathbf{U}_{10}$  at 10-m height

$$\tau_a = (\tau_x, \tau_y) = \rho_a C_d |U_{10}| \mathbf{U}_{10}, \quad (3)$$

$\rho_a$  is the air density, and  $C_d$  is the air-sea drag coefficient, which is related to  $U_{10}$  by the relation (Wu, 1982)

$$C_d = (0.8 + 0.065U_{10}) \times 10^{-3}. \quad (4)$$

When the effects of surface waves are considered, Ekman Eq. (1) and the boundary condition (2) are modified as follows (Jenkins, 1989; Raschle et al., 2006; Tang et al., 2007):

$$ifU_{WE} = \frac{\partial}{\partial z} \left( A_v \frac{\partial U_{WE}}{\partial z} \right) - ifU_s - T_{wds}, \quad (5)$$

$$A_v \frac{\partial U_{WE}}{\partial z} \Big|_{z=0} = \frac{\tau_a}{\rho_w} - \frac{\tau_{in}}{\rho_w}, \quad z = 0, \quad (6)$$

where  $U_s = u_s + iv_s$ ,  $U_{WE} = u_{WE} + iv_{WE}$ ,  $\mathbf{u}_s = (u_s, v_s)$  is the Stokes drift,  $\mathbf{u}_{WE} = (u_{WE}, v_{WE})$  is the quasi-Eulerian current, which is equal to the Lagrangian mean current minus the Stokes drift and can be understood as the Eulerian mean current as stated by Jenkins (1987a, 1989) and Perrie et al. (2003),  $\tau_{in}$  is the reduction of wind stress due to wave generation, and  $T_{wds}$  is the wave-induced

momentum transfer from waves to the mean flow due to dissipation of wave energy.

The lower boundary condition is taken as

$$U_{WE} \rightarrow 0 \quad (z \rightarrow -\infty). \quad (7)$$

Jenkins (1989) proposed the following forms for  $\tau_{in}$  and  $T_{wds}$  (also see Tang et al., 2007) calculated by the source terms from a directional spectral wave prediction model act to transfer momentum from the wave field to the current:

$$\tau_{in} = \tau_{inx} + i\tau_{iny} = \rho_w \int \left( \frac{\omega}{k} \right) K S_{in}(k, \theta) dk d\theta, \quad (8)$$

$$T_{wds} = T_{wdsx} + iT_{wdsy} = 2 \int \omega K e^{2kz} S_{ds}(k, \theta) dk d\theta, \quad (9)$$

where  $\omega$  is the angular frequency in rad/s,  $k$  is the modulus of the horizontal wavenumber vector  $\mathbf{k} = (k_x, k_y) = (k \cos \theta, k \sin \theta)$  given by the dispersion relation  $\omega^2 = gk$ ,  $\theta$  is the direction of the wave vector,  $K = k_x + ik_y$ ,  $S_{in}(k, \theta)$  is the wind input energy to waves,  $S_{ds}(k, \theta)$  is the wave energy lost by wave dissipation mechanisms as represented in third-generation WAM-type wave models (Hasselmann et al., 1988; Komen et al., 1994).

Following Kenyon (1969) and Huang (1971), the Stokes drift  $\mathbf{u}_s$  may be expressed as

$$\mathbf{u}_s = 2 \int \omega \mathbf{k} e^{2kz} E(k, \theta) dk d\theta, \quad (10)$$

where  $E(k, \theta)$  is the directional wavenumber spectrum of surface waves.

When waves are absent,  $E(k, \theta) = 0$ , the Stokes drift  $\mathbf{u}_s$  is zero, and  $S_{in}(k, \theta)$  and  $S_{ds}(k, \theta)$  also vanish. In this case, the wave-modified Ekman Eqs. (5)–(9), reduce to the usual Ekman relations, Eqs. (1)–(3). Taking  $\tau_{in} = T_{wds} = 0$ , the Eqs. (5) and (6) reduce to those of Lewis and Belcher (2004), which include only the effects of Stokes drift.

## 3. Solutions

### 3.1. Eddy viscosity independent of depth

As noted by Jenkins (1989), the Ekman surface current is directed at 45° to the right of the wind direction in the northern hemisphere if the eddy viscosity is assumed to be constant, which is inconsistent with the field observations of surface drift current, reviewed by Huang (1979) as stated in the introduction. In this section, we also assume that the eddy viscosity is independent of depth to study what the corresponding result is for the modified model. In fact, there are several approaches to estimate the vertical eddy diffusivity  $A_v$ . Many measurements have been made to determine its value, and different parameterizations have been proposed. A collection of values and functional forms can be found in Huang (1979) and Santiago-Mandujano and Firing (1990). When  $A_v$  is depth independent, we use the relationship between  $A_v$  and  $U_{10}$  first proposed by Ekman (1905) and confirmed by Santiago-Mandujano and Firing (1990)

$$A_v \equiv A_{v1} = 1.2 \times 10^{-4} U_{10}^2. \quad (11)$$

Thus, Eq. (5) can be rewritten as

$$A_{v1} \frac{d^2 U_{WE1}}{dz^2} - if U_{WE1} = if U_s + T_{wds}, \quad (12)$$

where  $U_{WE1}$  is the modified complex horizontal velocity corresponding to eddy diffusivity  $A_{v1}$ .

The general solution of (12) is

$$U_{WE1}(z) = A_1 e^{jz} + A_2 e^{-jz} + U_0(z), \quad (13)$$

where  $A_1$  and  $A_2$  are constants to be determined

$$j = \begin{cases} \frac{1}{d_e}(1+i), & f > 0, \\ \frac{1}{d_e}(1-i), & f < 0, \end{cases} \quad d_e = \sqrt{\frac{2A_{v1}}{|f|}}$$

is called the depth of the Ekman layer, and  $U_0(z)$  is a special solution of (12) as follows:

$$U_0(z) = \frac{1}{jA_{v1}} \int_{-\infty}^z \{if U_s(z') + T_{wds}(z')\} \sinh[j(z-z')] dz'. \quad (14)$$

The lower boundary condition (7) yields  $A_2 = 0$ , whilst the surface condition (6) reduces

$$A_1 = \frac{\tau_a - \tau_{in}}{j\rho_w A_{v1}} - \frac{1}{jA_{v1}} \int_{-\infty}^0 \{if U_s(z') + T_{wds}(z')\} \cosh(jz') dz', \quad (15)$$

and the corresponding wave-modified Ekman solution (13) can be written as

$$U_{WE1} = U_{E1} + U_{W1} \quad (16)$$

with

$$U_{E1} = \frac{\tau_a}{j\rho_w A_{v1}} e^{jz}, \quad (17)$$

$$U_{W1} = \left[ \frac{-\tau_{in}}{j\rho_w A_{v1}} - \frac{1}{jA_{v1}} \int_{-\infty}^0 \{if U_s(z') + T_{wds}(z')\} \cosh(jz') dz' \right] \times e^{jz} + U_0(z). \quad (18)$$

Thus, the wave-modified Ekman solution of (5) and (6) for depth-independent eddy viscosity can be viewed as the sum of two parts: the first one is the classical Ekman solution  $U_{E1}$ , and the second term  $U_{W1}$  represents the modification of wind-generated surface waves to the classical Ekman solution. This modification term depends on the choice of  $\tau_{in}$ , the Stokes drift  $U_s$ , wave dissipation  $T_{wds}$  and the eddy viscosity  $A_{v1}$ .

### 3.2. Eddy viscosity increasing linearly with depth

Although atmospheric turbulent boundary layers basically obey logarithmic velocity profiles, corresponding to a linear increase of eddy viscosity with height, it is very difficult to establish the presence of a log profile in a turbulent oceanic boundary layer because of surface waves and wave breaking. McWilliams et al. (1997) computed the eddy viscosity by using large eddy simulations of the ocean mixed layer, and demonstrated it follows a convex shape. Madsen (1977) examined the problem by taking the eddy viscosity increases linearly with depth throughout the mixed layer. That is,

$A_v = -\kappa u_* z$ , where  $\kappa = 0.4$  is von Karmen's constant and  $u_* = (|\tau_a|/\rho_w)^{1/2}$  is the oceanic friction velocity associated with the magnitude of the surface stress. One consequence of such linear variation  $A_v$  of with depth is the logarithmic singularity in the steady-state solution of (5) at  $z = 0$ . Madsen (1977) avoided this problem by introducing a sea surface roughness length scale  $z_{0s}$  and actually evaluating the 'surface' currents at  $z = -z_{0s}$ . Here, as Lewis and Belcher (2004) suggested, we introduce the sea surface roughness length into the eddy viscosity relation directly as follows:

$$A_v \equiv A_{v2} = -\kappa u_* (z - z_{0s}) = \kappa u_* (z_+ + z_{0s}), \quad (19)$$

where  $z_+ = -z > 0$ . This modified eddy viscosity relation still increases with depth, but it enables one to negate the log singularity at  $z = 0$  in a way that is mathematically consistent with the surface stress condition. It should be noted that the time independent linear profile used here can be considered an approximation for the profile of the eddy viscosity changes with wind speed as shown in the numerical model of Tang et al. (2007).

Substituting this form (19) of  $A_v$  into (5) and (6), we have

$$(z_+ + z_{0s}) \frac{\partial^2 U_{WE2}(-z_+)}{\partial z_+^2} + \frac{\partial U_{WE2}(-z_+)}{\partial z_+} - \frac{if}{\kappa u_*} U_{WE2}(-z_+) = \frac{[if U_s(-z_+) + T_{wds}(-z_+)]}{\kappa u_*}, \quad (20)$$

$$(z_+ + z_{0s}) \frac{\partial U_{WE2}(-z_+)}{\partial z_+} = -\frac{(\tau_a - \tau_{in})}{\rho_w \kappa u_*}, \quad z_+ = 0, \quad (21)$$

where  $U_{WE2}$  is the modified complex horizontal velocity corresponding to eddy diffusivity  $A_{v2}$ .

The general solution of (20) is

$$U_{WE2}(-z_+) = B_1 I_0 \left( 2 \sqrt{\frac{if(z_+ + z_{0s})}{\kappa u_*}} \right) + B_2 K_0 \left( 2 \sqrt{\frac{if(z_+ + z_{0s})}{\kappa u_*}} \right) + \Psi_0(-z_+), \quad (22)$$

where  $B_1$  and  $B_2$  are constants to be determined,  $I_0$  and  $K_0$  are the first and the second kinds of modified Bessel functions, respectively, and  $\Psi_0(-z_+)$  is a special solution of (20) as follows:

$$\Psi_0(-z_+) = -\frac{2}{\kappa u_*} \left\{ I_0 \left( 2 \sqrt{\frac{if(z_+ + z_{0s})}{\kappa u_*}} \right) \times \int_{z_+}^{+\infty} K_0 \left( 2 \sqrt{\frac{if(z' + z_{0s})}{\kappa u_*}} \right) [if U_s(-z') + T_{wds}(-z')] dz' - K_0 \left( 2 \sqrt{\frac{if(z_+ + z_{0s})}{\kappa u_*}} \right) \times \int_{z_+}^{+\infty} I_0 \left( 2 \sqrt{\frac{if(z' + z_{0s})}{\kappa u_*}} \right) [if U_s(-z') + T_{wds}(-z')] dz' \right\} \quad (23)$$

The boundary condition  $U_{WE2} \rightarrow 0$  as  $Z_+ \rightarrow \infty \Rightarrow B_1 = 0$ , whilst the surface condition (21) reduces

$$B_2 = -\frac{2(\tau_a - \tau_{in})}{\rho_w \kappa u_* \zeta_0 K'_0(\zeta_0)} + \frac{2}{\kappa u_*} \left\{ \frac{I'_0(\zeta_0)}{K'_0(\zeta_0)} \int_0^{+\infty} K_0(\zeta') [if U_s(-z') + T_{wds}(-z')] dz' - \int_0^{+\infty} I_0(\zeta') [if U_s(-z') + T_{wds}(-z')] dz' \right\}, \tag{24}$$

where  $\zeta' = 2\sqrt{if(z' + z_{0S})/\kappa u_*}$ ,  $\zeta_0 = 2\sqrt{if z_{0S}/\kappa u_*}$ ,  $I'_0$  and  $K'_0$ , respectively, are the derivatives of  $I_0$  and  $K_0$ .

Thus, the wave-modified Ekman solutions of (20) and (21) are

$$U_{WE2}(-Z_+) = U_{E2}(-Z_+) + U_{W2}(-Z_+), \tag{25}$$

with

$$U_{E2}(-Z_+) = -\frac{2\tau_a}{\rho_w \kappa u_* \zeta_0 K'_0(\zeta_0)} K_0(\zeta), \tag{26}$$

$$U_{W2}(-Z_+) = \frac{2\tau_{in}}{\rho_w \kappa u_* \zeta_0 K'_0(\zeta_0)} K_0(\zeta) + \frac{2}{\kappa u_*} \left\{ \frac{I'_0(\zeta_0)}{K'_0(\zeta_0)} K_0(\zeta) \int_0^{+\infty} K_0(\zeta') \times [if U_s(-z') + T_{wds}(-z')] dz' - K_0(\zeta) \int_0^{Z_+} I_0(\zeta') [if U_s(-z') + T_{wds}(-z')] dz' - I_0(\zeta) \int_{Z_+}^{+\infty} K_0(\zeta') [if U_s(-z') + T_{wds}(-z')] dz' \right\} \tag{27}$$

In a similar manner to that of the previous section, these wave-modified Ekman solutions with  $A_v \equiv A_{v2} = -\kappa u_*(z - z_{0S})$  also can be viewed as the sum of two parts: one is the classical Ekman solution  $U_{E2}$ , and the other,  $U_{W2}$ , represents the modification of wind-generated surface waves to the classical Ekman solution, which depends on the choice of  $\tau_{in}$ ,  $U_s$  and  $T_{wds}$ .

When the influence of surface waves is neglected, then  $U_{W1} = U_{W2} = 0$ , and modified complex horizontal velocities, both  $U_{WE1}$  and  $U_{WE2}$ , reduce to the usual Ekman velocity  $U_E$ . If only the Stokes drift  $U_s$  is kept, and the effects of  $\tau_{in}$  and  $T_{wds}$  are ignored (namely, taking  $\tau_{in} = T_{wds} = 0$ ), the solutions (16) and (25) reduced to those of Lewis and Belcher (2004).

#### 4. Illustrative examples

As illustrative examples of the effects of random surface waves on the Ekman current, we calculated  $u_E$ ,  $v_E$ ,  $u_{WE}$  and  $v_{WE}$  for various wind speeds by taking  $\rho_a = 1.2 \text{ kg m}^{-3}$ ,  $\rho_w = 1025 \text{ kg m}^{-3}$ ,  $f = 10^{-4} \text{ s}^{-1}$  for a fully developed wind-generated sea described by the wave-number spectrum of Donelan and Pierson (1987),

$$E(k, \theta) = \frac{0.00162 \times U_{10}}{k^{2.5} g^{0.5}} \exp\left(-\frac{g^2}{k^2 (1.2U_{10})^4}\right) 1.7^\Gamma \times \mu\left(\frac{k}{k_p}\right) \text{sech}^2\left[\mu\left(\frac{k}{k_p}\right)\theta\right] \quad (0 < k < \infty, -\pi < \theta < \pi), \tag{28}$$

where  $\theta$  is the wave direction relative to the wind (the direction of wind is assumed to be along the x-axis) and

$$\Gamma = \exp\left\{-1.22 \left[\frac{1.2U_{10}k^{0.5}}{g^{0.5}} - 1\right]^2\right\}, \tag{29}$$

$$\mu\left(\frac{k}{k_p}\right) = \begin{cases} 1.24, & 0 < k/k_p < 0.31, \\ 2.61(k/k_p)^{0.65}, & 0.31 < k/k_p < 0.9, \\ 2.28(k_p/k)^{0.65}, & 0.9 < k/k_p < 10. \end{cases} \tag{30}$$

The peak of the spectrum is given by

$$k_p = \frac{g}{(1.2U_{10})^2}. \tag{31}$$

$S_{in}$  is specified by the Hasselmann et al. (1988) in the WAM wave model formulation for wind input energy to waves:

$$S_{in}(k, \theta) = \beta E(k, \theta), \tag{32}$$

where

$$\beta = \max\left[0, 0.25 \frac{\rho_a}{\rho_w} \left(28 \frac{u_a^q}{C} \cos\theta - 1\right)\right] \omega, \tag{33}$$

in which  $u_a^q = \sqrt{C_d}|U_{10}|$  is the air friction velocity, and the phase velocity is given by  $C = \omega/k$ . The dissipation source function is taken as follows (Hasselmann et al., 1988; Komen et al., 1994):

$$S_{ds}(k, \theta) = -2.25 \langle \omega \rangle (\langle k \rangle^2 m_0)^2 \left(\frac{k}{\langle k \rangle} + \left(\frac{k}{\langle k \rangle}\right)^2\right) E(k, \theta), \tag{34}$$

where

$$m_0 = \iint E(k, \theta) dk d\theta, \tag{35}$$

$$\langle \omega \rangle = \left[m_0^{-1} \iint E(k, \theta) \omega^{-1} dk d\theta\right]^{-1}, \tag{36}$$

$$\langle k \rangle = \left[m_0^{-1} \iint E(k, \theta) k^{-1/2} dk d\theta\right]^{-2}. \tag{37}$$

It should be noted that there is considerably uncertainty about this form of dissipation term and its behaviour at high frequencies (see Komen et al., 1994).

Using (8)–(10), (32), (34), (3), and noting that  $E(k, \theta) = E(k, -\theta)$ , we have

$$v_s = \tau_{ay} = \tau_{iny} = T_{wdsy} = 0, \tag{38}$$

$$u_s(z) = 4\sqrt{g} \int_0^\infty \int_0^\pi k^{3/2} e^{2kz} \cos(\theta) E(k, \theta) d\theta dk, \tag{39}$$

$$\tau_{ax} = \rho_a C_d U_{10}^2, \tag{40}$$

$$\tau_{inx} = 2\rho_w \sqrt{g} \int_0^\infty \int_0^\pi k^{1/2} \beta \cos(\theta) E(k, \theta) d\theta dk, \tag{41}$$

$$T_{wdsx}(z) = 4\sqrt{g} \int_0^\infty \int_0^\pi k^{3/2} \cos(\theta) e^{2kz} S_{ds}(k, \theta) d\theta dk. \tag{42}$$

Numerical results of  $\tau_{ax}$ ,  $\tau_{inx}$ ,  $d_e$  and  $u_s(0)$  for various wind speed values of  $U_{10}$  are shown in Table 1.

4.1. Eddy viscosity independent of depth

For constant eddy viscosity presented by (11), the real and imaginary parts of the corresponding complex solutions (16)–(18) can be rewritten as (see Appendix A)

$$u_{WE1} = u_{E1} + u_{W1}, \tag{43}$$

$$v_{WE1} = v_{E1} + v_{W1}, \tag{44}$$

where  $u_{E1}$  and  $v_{E1}$  denote the classical Ekman current,  $u_{W1}$  and  $v_{W1}$  are the modifications due to the Stokes drift  $U_s$ , wind input  $\tau_{in}$  and wave dissipation  $T_{wds}$ .

When the effects of wind input and wave dissipation are negligible, i.e.,  $\tau_{in} = T_{wds} = 0$ , the solutions of  $u_{WE1}$  and  $v_{WE1}$  reduce to those of Lewis and Belcher (2004), and we write them as  $u_{SE1}$  and  $v_{SE1}$ , respectively. The behaviour of  $u_{E1}$ ,  $v_{E1}$ ,  $u_{SE1}$ ,  $v_{SE1}$ ,  $u_{WE1}$ ,  $v_{WE1}$ ,  $|u_{E1}|$ ,  $|u_{SE1}|$  and  $|u_{WE1}|$  for wind speeds  $U_{10} = 10$  and 20 m/s are shown in Figs. 1–6.

From the above figures we could not see any significant impact of including the wind input and wave dissipation through the terms involving  $S_{in}$  and  $S_{ds}$  to modeling of surface currents. As we know, the angular turning of the classical Ekman surface current is  $45^\circ$  for the above depth-independent constant eddy viscosity. However, if we only introduce the Stokes drift in the momentum equation

**Table 1**  
 $\tau_{ax}$ ,  $\tau_{inx}$ ,  $d_e$ , and  $u_s(0)$  for different wind speeds  $U_{10}$ .

$U_{10}$ ( $\text{m s}^{-1}$ )	5	10	15	20	25	30
$\tau_{ax}$ (Pa)	0.0338	0.1740	0.4793	1.0080	1.8187	2.9700
$\tau_{inx}$ (Pa)	0.0060	0.0378	0.1176	0.2675	0.5077	0.8564
$d_e$ (m)	7.7460	15.492	23.238	30.984	38.730	46.476
$u_s(0)$ ( $\text{m s}^{-1}$ )	0.0593	0.1187	0.1780	0.2373	0.2967	0.3560

without considering wind input and wave dissipation as Lewis and Belcher (2004) and Polton et al. (2005) did, the angular turning will increase to  $56.0^\circ$  and  $56.9^\circ$ , respectively, for  $U_{10} = 10$  and 20 m/s. These results are qualitatively in agreement with those reported by Lewis and Belcher (2004) and Polton et al. (2005). If the Stokes drift, wind input and wave dissipation are introduced, the angular turning increased to  $56.8^\circ$  and  $60.3^\circ$ , respectively. These results show that the effects of the wind input and wave dissipation on surface current are small, relative to the impact of the Stokes drift. Especially in the case of high wind speeds  $U_{10} = 20$  m/s (see Figs. 4–6), the effects of the wind input and wave dissipation on the profiles of the classical Ekman current are negligible, which lead to

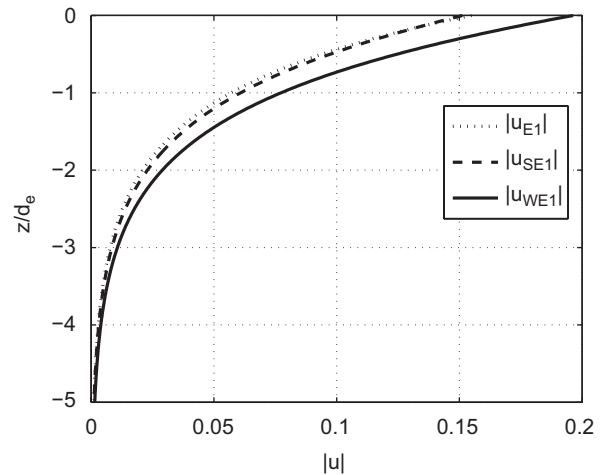


Fig. 2.  $|u_{E1}|$ ,  $|u_{SE1}|$  and  $|u_{WE1}|$  for wind speed  $U_{10} = 10$  m/s.

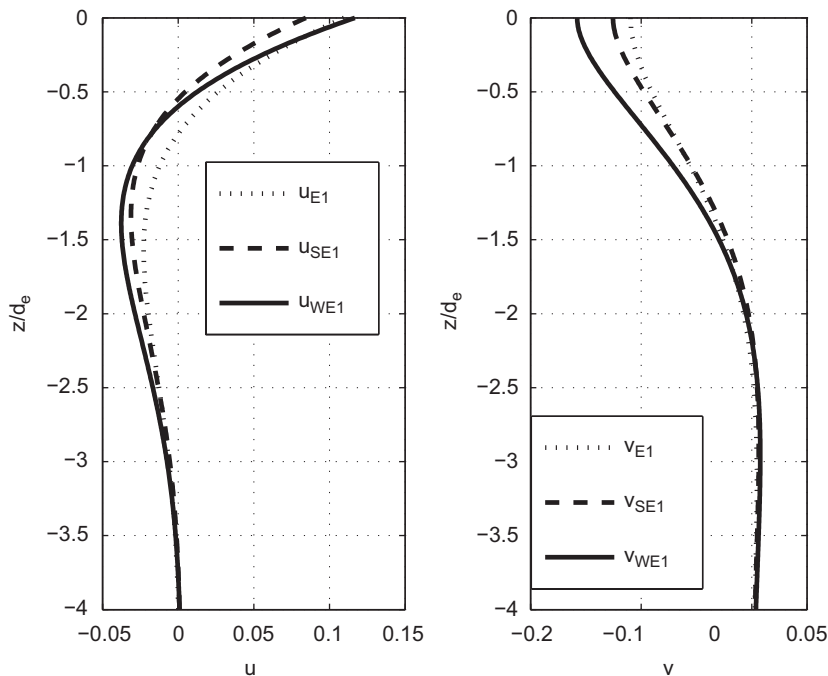


Fig. 1.  $u_{E1}$ ,  $v_{E1}$ ,  $u_{SE1}$ ,  $v_{SE1}$ ,  $u_{WE1}$  and  $v_{WE1}$  for wind speed  $U_{10} = 10$  m/s.

the solutions proposed in this paper approach those of Lewis and Belcher (2004) at high wind speeds.

4.2. Eddy viscosity increasing linearly with depth

For the eddy viscosity increasing linearly with depth as presented by (19), the real and imaginary parts of the corresponding complex horizontal velocity presented by (25)–(27) can be rewritten as (see Appendix A)

$$u_{WE2} = u_{E2} + u_{W2}, \tag{45}$$

$$v_{WE2} = v_{E2} + v_{W2}. \tag{46}$$

The expressions of  $u_{E2}$ ,  $v_{E2}$ ,  $u_{W2}$  and  $v_{W2}$  are presented in Appendix A. The sea surface roughness length scale  $z_{0S}$  appearing in the above expressions must be chosen before the calculation. Lewis and Belcher (2004) took

$$z_{0S} = \frac{\kappa u_*}{4f} \exp\left(-\frac{q\kappa U_{10}}{u_*}\right), \tag{47}$$

where  $q = 0.01–0.04$  is the relative strength of the current relative to the wind. For  $q = 0.02$  and  $f = 10^{-4}$ , the values of  $z_{0S}$  calculated by (47) are 0.0054, 0.0281, 0.0841, 0.1908, 0.3652 and 0.6233, respectively, for  $U_{10} = 5, 10, 15, 20, 25$  and 30 m/s. These values are two orders of magnitude

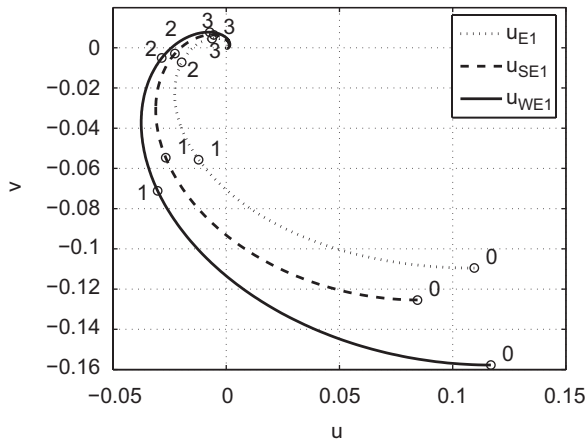


Fig. 3. Hodograph showing the depth dependence of  $u_{E1}$ ,  $u_{SE1}$  and  $u_{WE1}$  for  $U_{10} = 10$  m/s. The numbers on the graph denote dimensionless depth of  $-z/d_e$ .

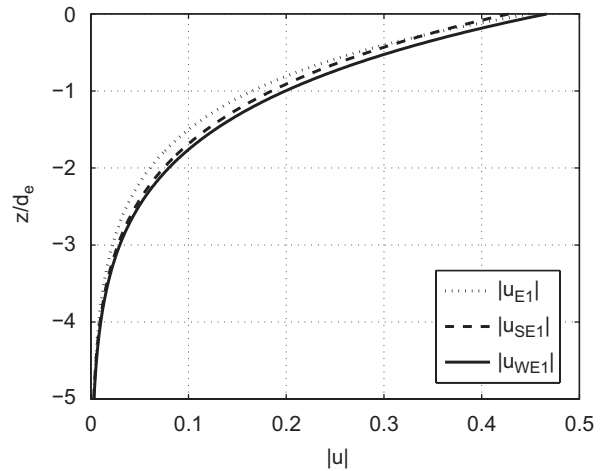


Fig. 5. As Fig. 2, but for  $U_{10} = 20$  m/s.

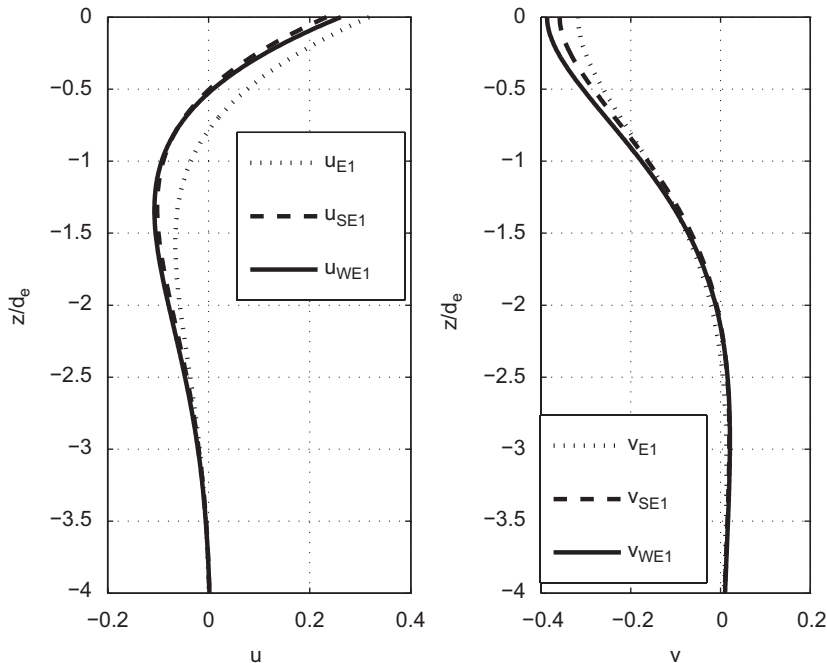


Fig. 4. As Fig. 1, but for  $U_{10} = 20$  m/s.

below that used by Raschle et al. (2006) who parameterize  $z_{0S}$  as the order of the significant wave height  $H_s$  as in Terray et al. (1999). There are still many discussions on the actual value of  $z_{0S}$  (Gemrich and Farmer, 2004; Raschle et al., 2006). Here,  $z_{0S}$  is taken as a more realistic value of  $z_{0S} \approx 0.85H_s$  as Mellor and Blumberg (2004) suggested, that is

$$z_{0S} = 665 \left( \frac{c_p}{u_*^2} \right)^{1.5} \frac{u_*^2}{g} = 665 \left( \frac{1.2}{\sqrt{C_d}} \right)^{1.5} \frac{u_*^2}{g}, \quad (48)$$

The values of  $z_{0S}$  calculated by (48) are 0.4779, 2.0368, 4.8204, 8.9375, 14.4764 and 21.5119 for  $U_{10} = 5, 10, 15, 20, 25$  and  $30$  m/s, respectively.

The solutions presented by (45) and (46) are calculated for various wind speeds by using polynomial approximations cited by Abramowitz and Stegun (1964) for Kelvin functions, and behaviours of  $u_{E2}, v_{E2}, u_{SE2}, v_{SE2}, u_{WE2}, v_{WE2}, |u_{E2}|, |u_{SE2}|$  and  $|u_{WE2}|$  for wind speeds  $U_{10} = 10$  and  $20$  m/s are shown in Figs. 7–12.

Compared to the results of previous section, it is noted that the vertical structure of eddy viscosity is very important to modeling of the surface current. When the eddy viscosity increases linearly with depth, the angular turning of the modified Ekman surface current will increase to  $38.1^\circ$  from  $25.9^\circ$  of the classical Ekman current for  $U_{10} = 10$  m/s, and to  $44.7^\circ$  from  $28.2^\circ$  for  $U_{10} = 20$  m/s. If only the Stokes drift term is included, the angular turning will increase to  $35.6^\circ$  and  $40.6^\circ$ ,

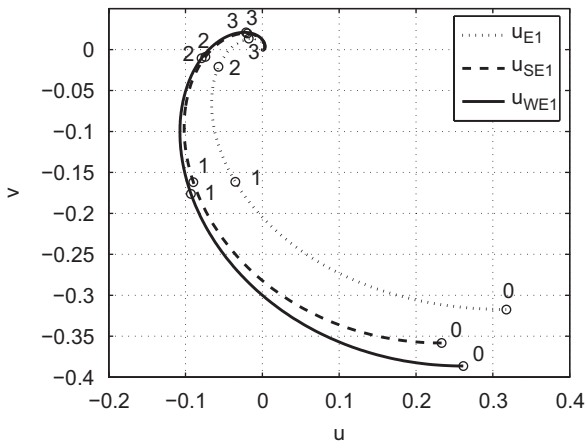


Fig. 6. As Fig. 3, but for  $U_{10} = 20$  m/s.

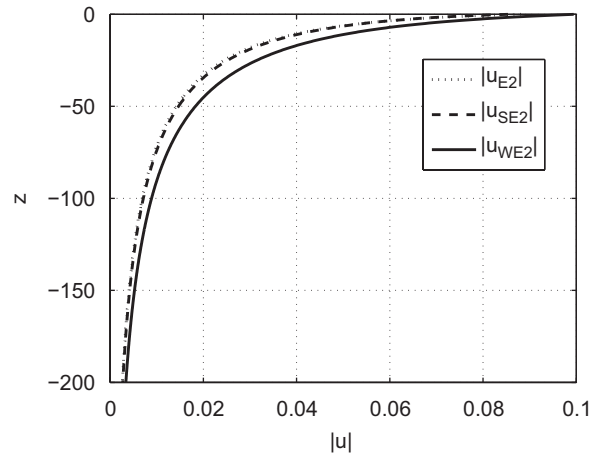


Fig. 8.  $|u_{E2}|, |u_{SE2}|$  and  $|u_{WE2}|$  for wind speed  $U_{10} = 10$  m/s.

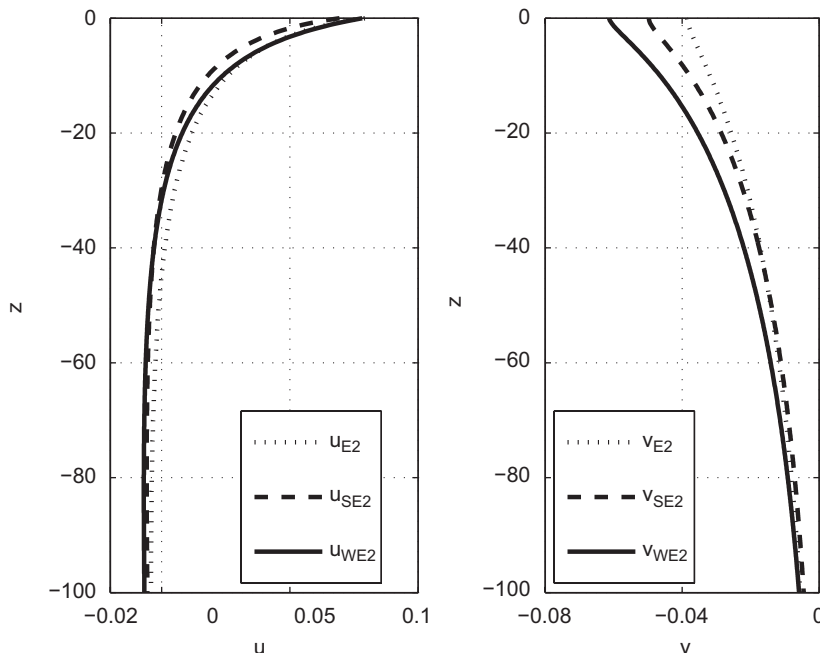
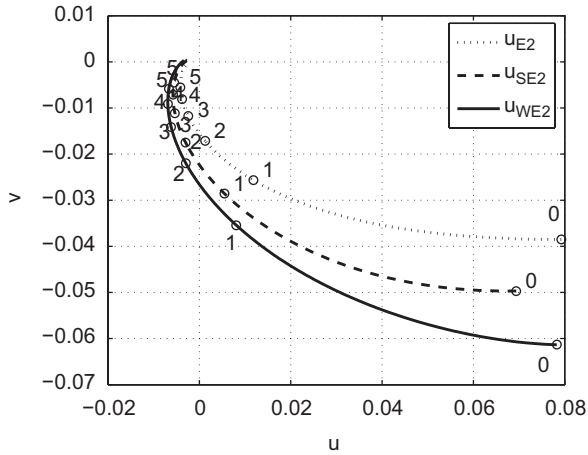


Fig. 7.  $u_{E2}, v_{E2}, u_{SE2}, v_{SE2}, u_{WE2}$  and  $v_{WE2}$  for wind speed  $U_{10} = 10$  m/s.

respectively. These results also confirm that the effects of the wind input and wave dissipation on surface current are small, relative to the impact of the Stokes drift. Especially, as shown in Figs. 10–12 for high wind speeds ( $U_{10} = 20$  m/s), the effects of the wind input and wave dissipation on the profiles of the classical Ekman current are negligible, which lead to the solutions proposed in this paper approach those of Lewis and Belcher (2004) at high wind speeds. These results agree with the analysis of a numerical model and surface current data by Tang et al. (2007).

### 5. Comparisons with the observations

Extracting the mean wind-driven current profile from the background of wave orbital motions, inertial oscillations, and geostrophic eddies requires sophisticated and sensitive instruments that can be deployed for long periods. Consequently it is only relatively recently that data have been collected that can be compared with models of the wind-driven current profile, and there are relatively few such data. Here, as Polton et al. (2005), we use two sets of data reported by Price and Sundermeyer (1999), namely the Long-Term Upper-Ocean Study (LOTUS3) and the Eastern Boundary Current (EBC) data to compare with our model results. The LOTUS3 data were



**Fig. 9.** Hodograph showing the depth dependence of  $u_{E2}$ ,  $u_{SE2}$  and  $u_{WE2}$  for  $U_{10} = 10$  m/s. The numbers from 0 to 5 appeared on the graph are, respectively, corresponding to the depths of  $z = 0, -20, -40, -60, -80$  and  $-100$  m.

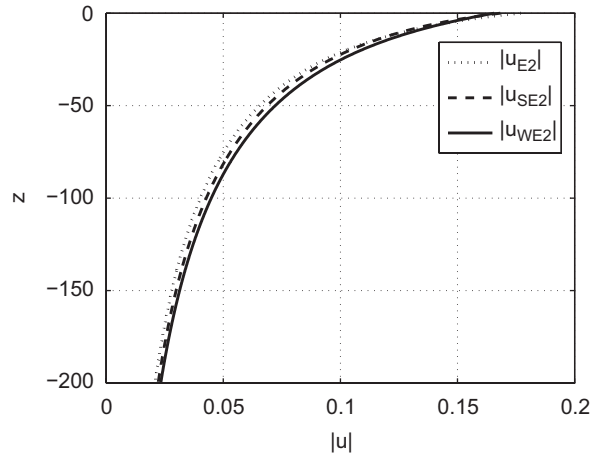


**Fig. 11.** As Fig. 8, but for  $U_{10} = 20$  m/s.

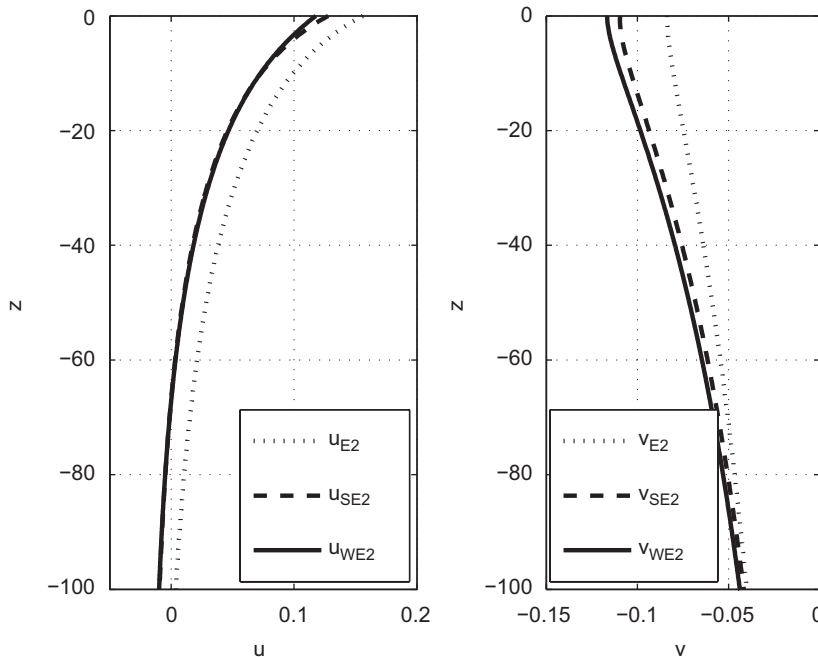


**Fig. 10.** As Fig. 7, but for  $U_{10} = 20$  m/s.

collected in the western Sargasso Sea (34°N, 70°W) spanning 160 days during the summer months of 1982. The average wind stress for this dataset is reported to be 0.07 Pa. The eastern boundary current (EBC) data were taken from a mooring 400 km off the coast of North California (37°N, 128°W) and were collected over a 6-month period from 8 April to 20 October 1993 using

ADCP and buoy wind observations. The average wind stress for this dataset is reported to be 0.09 Pa. Observed time averaged Ekman current magnitudes and deflection angles for these two datasets were estimated and summarized in Table 2 by Lewis and Belcher (2004) from the hodographs and three-dimensional profiles shown in Fig. 1 of Price and Sundermeyer (1999), and will be used here. Fig. 13 shows the observed current profiles of two datasets. The solutions presented by (45) and (46) for the eddy viscosities of (19) are also shown to compare with these two observations. For the LOTUS3 comparison, the solution is obtained by using  $U_{10} = 6.8$  m/s and  $f = 8.36 \times 10^{-5} \text{ s}^{-1}$ . For the EBC comparison,  $U_{10} = 7.6$  m/s and  $f = 8.77 \times 10^{-5} \text{ s}^{-1}$  are used. Here, the wind speeds  $U_{10} = 6.8$  and 7.6 m/s are estimated from Eqs. (3) and (4) for  $\tau_a = 0.07$  and 0.09 Pa ( $\rho_a = 1.2 \text{ kg m}^{-3}$ ), respectively. It is noted that these values of  $U_{10}$  are little larger than those presented by Lewis and Belcher (2004).

The profiles of Fig. 13 show that there are considerable deviations from the classical Ekman profiles, which Price and Sundermeyer (1999) attribute to dynamical effects of mixed layer stratification and diurnal variations in the mixed layer depth. However, the comparisons between observations and the theoretical predictions as show in Fig. 13, demonstrate that inclusion of the Stokes drift, wind input and wave dissipation can largely reduce these

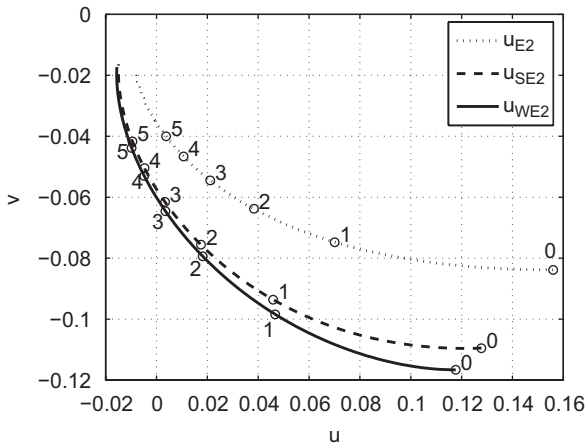


Fig. 12. As Fig. 9, but for  $U_{10} = 20$  m/s.

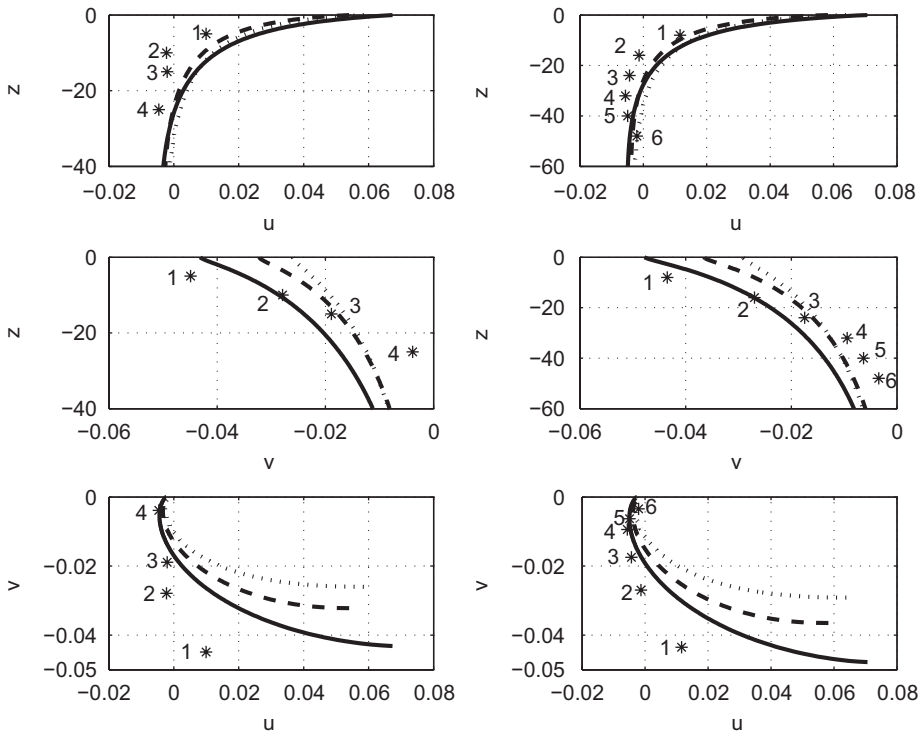


Fig. 13. The comparison of the model results with the LOTUS3 (left) and EBC (right) data, denoted with star. The depths of the experimental data points are marked by the numbers. The numbers from 1 to 4 appeared on the left panel subfigures are, respectively, corresponding to the depths of  $z = -5, -10, -15$  and  $-25$  m, and the numbers from 1 to 6 appeared on the right panel subfigures are, respectively, corresponding to the depths of  $z = -8, -16, -24, -32, -40$  and  $-48$  m. The dotted lines are the classical Ekman solutions ( $u_{E2}, v_{E2}$ ), the dashed lines are the solutions ( $u_{SE2}, v_{SE2}$ ) which only including the Stokes drift, the solid lines are the solutions ( $u_{WE2}, v_{WE2}$ ) which including the Stokes drift, wind input and wave dissipation. The top panel depicts the downward velocities as functions of depth, and the middle panel shows the crosswind, respectively. The bottom panels depict hodographs that display the downwind velocity plotted against the crosswind velocity.

discrepancies. Especially, as stated by Lewis and Belcher (2004), the inclusion of the Stokes drift obviously reconcile the discrepancies in the angular deflections of the steady-state currents. This leads to the conclusion that Ekman layer currents are significantly influenced by the surface waves. But, the model still gives relatively poor fits to the data because the spirals are too spread out and not flattened in that the sense that the currents decay more rapidly as the current rotates to the right. This flattening of the spirals may be brought about by stratification or many other contributions discussed next section. It should be noted that the diagram obtained by Lewis and Belcher (2004) better fits to the data than those shown here in Fig. 13, because in their model they employed a no slip boundary condition at a finite depth (not Eq. (7)), to try and replicate the attenuation of the spirals brought about by stratification effects. This may not be the physically correct way to incorporate stratification but it is an effective way of modelling its effects.

### 6. Conclusions and discussion

The effects of random surface waves on the standard Ekman surface current are considered based on the approach of Jenkins (1989) and Tang et al. (2007) by including the momentum effects of Stokes drift, the input of momentum into waves by a steady wind, and the partial conversion of wave dissipation momentum into the current field. Analytic steady solutions are obtained for wave-modified Ekman equations when the eddy viscosity coefficient is, respectively, taken as depth-independent and proportional to depth. The solutions presented depend on the two-dimensional wavenumber spectrum of ocean waves, wind speed, the Coriolis parameter and the densities of air and water, and they reduce to those of Lewis and Belcher (2004) if only the Stokes drift is included in the model. As illustrative examples, we considered a fully developed wind-generated sea for various wind speeds. Wave-modified current profiles were calculated and compared with the classical Ekman theory and Lewis and Belcher's (2004) modification by using the Donelan and Pierson (1987) wavenumber spectrum, the WAM wave model formulation for wind input energy to waves, and wave energy dissipation converted to currents. The main conclusion of our research is that: Ekman layer currents are significantly influenced by the surface waves, but the effects of the wind input and wave dissipation on surface current are small, relative to the impact of the Stokes drift. Illustrative examples for a fully developed sea show that the wave-modified Ekman current will increase the angular turning of the classical Ekman surface current greatly, mainly due to the Stokes drift as stated by Lewis and Belcher (2004), Polton et al. (2005) and Saetra and Albretsen (2007), especially at high wind speeds. The comparisons between observations and the theoretical predictions demonstrate that inclusion of the Stokes drift, wind input and wave dissipation can largely reduce the discrepancies between the classical Ekman theory and

the observations. But, the model still gives relatively poor fits to the observational data, and further careful research is necessary.

It is noted that the corresponding solutions can be obtained by using the wave spectrum from the wave model for a more general developing sea, although we only illustrate the current profiles for a fully developed wind-generated sea as examples. Furthermore, the steady solutions presented in the paper may be extended to the time-dependent cases using a Laplace transform technique analogous to that of Lewis and Belcher (2004) in the study of the effects of the Stokes drift on Ekman current. It is also noted that we neglected many other contributions to Ekman surface currents, for example, density stratification, surface heating, buoyancy flux and the horizontal component of the Coriolis frequency. These effects can be important in certain situations and should be considered for accurate modeling of surface currents, but are also beyond the scope of the present study. Especially, as Price and Sundermeyer (1999) and Raschle (2007) demonstrated, variable surface buoyancy fluxes and near-surface stratification have a significant impact on the Ekman layer. It is therefore of obvious importance to extend the present study to the stratified condition. Furthermore, the parameterization forms of wave-current interactions involving  $S_{in}$  and  $S_{ds}$  also affected the presented solutions, which should be further investigated, and the theoretical solutions should be further verified by field observations.

### Appendix A. Real and imaginary parts of $U_{WE1}$ and $U_{WE2}$

For constant eddy viscosity presented by (11), the real and imaginary parts of the corresponding complex solutions  $U_{WE1}$  presented by (16)–(18) can be written as

$$u_{WE1} = u_{E1} + u_{W1}, \tag{A.1}$$

$$v_{WE1} = v_{E1} + v_{W1}, \tag{A.2}$$

where the classical Ekman current  $u_{E1}$  and  $v_{E1}$  are

$$u_{E1} = \frac{\rho_a C_d d_e}{2\rho_w c_0} \left[ \cos\left(\frac{z}{d_e}\right) + \sin\left(\frac{z}{d_e}\right) \right] e^{z/d_e}, \tag{A.3}$$

$$v_{E1} = \frac{\rho_a C_d d_e}{2\rho_w c_0} \left[ \sin\left(\frac{z}{d_e}\right) - \cos\left(\frac{z}{d_e}\right) \right] e^{z/d_e}, \tag{A.4}$$

and the modifications to  $u_{E1}$  and  $v_{E1}$  are

$$\begin{aligned} u_{W1} = & -\frac{\tau_{inx} d_e}{2\rho_w c_0 U_{10}^2} \left[ \cos\left(\frac{z}{d_e}\right) + \sin\left(\frac{z}{d_e}\right) \right] e^{z/d_e} \\ & + \frac{d_e}{2c_0 U_{10}^2} \left\{ \left[ \sin\left(\frac{z}{d_e}\right) - \cos\left(\frac{z}{d_e}\right) \right] \right. \\ & \times \int_{-\infty}^0 \left[ f u_s(z') \cosh\left(\frac{z'}{d_e}\right) \cos\left(\frac{z'}{d_e}\right) \right. \\ & \left. \left. + T_{wdsx}(z') \sinh\left(\frac{z'}{d_e}\right) \sin\left(\frac{z'}{d_e}\right) \right] dz' \right\} \end{aligned}$$

$$\begin{aligned}
 & + \left[ \cos\left(\frac{z}{d_e}\right) + \sin\left(\frac{z}{d_e}\right) \right] \int_{-\infty}^0 \left[ f u_s(z') \sinh\left(\frac{z'}{d_e}\right) \sin\left(\frac{z'}{d_e}\right) \right. \\
 & - T_{wdsx}(z') \cosh\left(\frac{z'}{d_e}\right) \cos\left(\frac{z'}{d_e}\right) \left. \right] dz' \Big\} e^{z/d_e} \\
 & + \frac{d_e}{2c_0 U_{10}^2} \int_{-\infty}^z \left\{ [f u_s(z') + T_{wdsx}(z')] \right. \\
 & \times \sinh\left(\frac{z-z'}{d_e}\right) \cos\left(\frac{z-z'}{d_e}\right) \\
 & \left. + [T_{wdsx}(z') - f u_s(z')] \cosh\left(\frac{z-z'}{d_e}\right) \sin\left(\frac{z-z'}{d_e}\right) \right\} dz',
 \end{aligned} \tag{A.5}$$

$$\begin{aligned}
 v_{W1} = & - \frac{\tau_{inx} d_e}{2\rho_w c_0 U_{10}^2} \left[ \sin\left(\frac{z}{d_e}\right) - \cos\left(\frac{z}{d_e}\right) \right] e^{z/d_e} \\
 & - \frac{d_e}{2c_0 U_{10}^2} \left\{ \left[ \cos\left(\frac{z}{d_e}\right) + \sin\left(\frac{z}{d_e}\right) \right] \right. \\
 & \times \int_{-\infty}^0 \left[ f u_s(z') \cosh\left(\frac{z'}{d_e}\right) \cos\left(\frac{z'}{d_e}\right) \right. \\
 & \left. + T_{wdsx}(z') \sinh\left(\frac{z'}{d_e}\right) \sin\left(\frac{z'}{d_e}\right) \right] dz' \\
 & + \left[ \cos\left(\frac{z}{d_e}\right) - \sin\left(\frac{z}{d_e}\right) \right] \\
 & \times \int_{-\infty}^0 \left[ f u_s(z') \sinh\left(\frac{z'}{d_e}\right) \sin\left(\frac{z'}{d_e}\right) \right. \\
 & \left. - T_{wdsx}(z') \cosh\left(\frac{z'}{d_e}\right) \cos\left(\frac{z'}{d_e}\right) \right] dz' \Big\} e^{z/d_e} \\
 & + \frac{d_e}{2c_0 U_{10}^2} \int_{-\infty}^z \left\{ [f u_s(z') - T_{wdsx}(z')] \right. \\
 & \times \sinh\left(\frac{z-z'}{d_e}\right) \cos\left(\frac{z-z'}{d_e}\right) \\
 & \left. + [T_{wdsx}(z') + f u_s(z')] \cosh\left(\frac{z-z'}{d_e}\right) \sin\left(\frac{z-z'}{d_e}\right) \right\} dz',
 \end{aligned} \tag{A.6}$$

where  $c_0 = 1.2 \times 10^{-4}$ .

For the eddy viscosity increasing linearly with depth as presented by (19), the real and imaginary parts of the corresponding complex horizontal velocity  $U_{WE2}$  presented by (25)–(27) can be written as

$$u_{WE2}(-z_+) = u_{E2}(-z_+) + u_{W2}(-z_+), \tag{A.7}$$

$$v_{WE2}(-z_+) = v_{E2}(-z_+) + v_{W2}(-z_+), \tag{A.8}$$

with

$$u_{E2}(-z_+) = - \frac{2\tau_{ax}}{\rho_w \kappa u_* x_0 F_0} [Ker(x)Ker'(x_0) + Kei(x)Kei'(x_0)], \tag{A.9}$$

$$v_{E2}(-z_+) = - \frac{2\tau_{ax}}{\rho_w \kappa u_* x_0 F_0} [Kei(x)Ker'(x_0) - Ker(x)Kei'(x_0)], \tag{A.10}$$

$$\begin{aligned}
 u_{W2}(-z_+) = & \frac{2\tau_{inx}}{\rho_w \kappa u_* x_0 F_0} [Ker(x)Ker'(x_0) + Kei(x)Kei'(x_0)] \\
 & + \frac{2}{\kappa u_*} \left\{ \frac{F_2}{F_0} \int_0^{+\infty} ([Ker(x)Ker'(x') - Kei(x)Kei'(x')] T_{wdsx}(-z') \right. \\
 & \left. - f [Ker(x)Kei(x') + Kei(x)Ker'(x')] u_s(-z') \right\} dz'
 \end{aligned}$$

$$\begin{aligned}
 & - \frac{F_1}{F_0} \int_0^{+\infty} ([Ker(x)Kei(x') + Kei(x)Ker'(x')] T_{wdsx}(-z') \\
 & + f [Ker(x)Ker'(x') - Kei(x)Kei'(x')] u_s(-z')) dz' \\
 & - Ker(x) \int_0^{z_+} [Ber(x') T_{wdsx}(-z') - f Bei(x') u_s(-z')] dz' \\
 & + Kei(x) \int_0^{z_+} [f Ber(x') u_s(-z') + Bei(x') T_{wdsx}(-z')] dz' \\
 & - Ber(x) \int_{z_+}^{+\infty} [Ker(x') T_{wdsx}(-z') - f Kei(x') u_s(-z')] dz' \\
 & + Bei(x) \int_{z_+}^{+\infty} [Kei(x') T_{wdsx}(-z') + f Ker(x') u_s(-z')] dz' \Big\},
 \end{aligned} \tag{A.11}$$

$$\begin{aligned}
 v_{W2}(-z_+) = & \frac{2\tau_{inx}}{\rho_w \kappa u_* x_0 F_0} [Kei(x)Ker'(x_0) - Ker(x)Kei'(x_0)] \\
 & + \frac{2}{\kappa u_*} \left\{ \frac{F_1}{F_0} \int_0^{+\infty} ([Ker(x)Ker'(x') - Kei(x)Kei'(x')] T_{wdsx}(-z') \right. \\
 & - f [Ker(x)Kei(x') + Kei(x)Ker'(x')] u_s(-z')) dz' \\
 & + \frac{F_2}{F_0} \int_0^{+\infty} ([Ker(x)Kei(x') + Kei(x)Ker'(x')] T_{wdsx}(-z') \\
 & + f [Ker(x)Ker'(x') - Kei(x)Kei'(x')] u_s(-z')) dz' \\
 & - Kei(x) \int_0^{z_+} [Ber(x') T_{wdsx}(-z') - f Bei(x') u_s(-z')] dz' \\
 & - Ker(x) \int_0^{z_+} [f Ber(x') u_s(-z') + Bei(x') T_{wdsx}(-z')] dz' \\
 & - Bei(x) \int_{z_+}^{+\infty} [Ker(x') T_{wdsx}(-z') - f Kei(x') u_s(-z')] dz' \\
 & \left. - Ber(x) \int_{z_+}^{+\infty} [Kei(x') T_{wdsx}(-z') + f Ker(x') u_s(-z')] dz' \right\},
 \end{aligned} \tag{A.12}$$

where  $x_0 = 2\sqrt{fz_{05}/\kappa u_*}$ ,  $x = 2\sqrt{f(z_+ + z_{05})/\kappa u_*}$ ,  $x' = 2\sqrt{f(z' + z_{05})/\kappa u_*}$ , *Ber*, *Bei*, *Ker* and *Kei* are Kelvin functions, they and their derivatives *Ber'*, *Bei'*, *Ker'* and *Kei'* are defined by Abramowitz and Stegun (1964)

$$I_0(x\sqrt{i}) = Ber(x) + iBei(x), \tag{A.13}$$

$$K_0(x\sqrt{i}) = Ker(x) + iKei(x), \tag{A.14}$$

$$I'_0(x\sqrt{i}) = \frac{\sqrt{2}}{2} \{Ber'(x) + Bei'(x) - i[Ber'(x) - Bei'(x)]\}, \tag{A.15}$$

$$K'_0(x\sqrt{i}) = \frac{\sqrt{2}}{2} \{Ker'(x) + Kei'(x) - i[Ker'(x) - Kei'(x)]\}, \tag{A.16}$$

and

$$F_0 = [Ker'(x_0)]^2 + [Kei'(x_0)]^2, \tag{A.17}$$

$$F_1 = Bei'(x_0)Ker'(x_0) - Ber'(x_0)Kei'(x_0), \tag{A.18}$$

$$F_2 = Ber'(x_0)Ker'(x_0) + Bei'(x_0)Kei'(x_0). \tag{A.19}$$

**References**

Abramowitz, M., Stegun, I.A., 1964. Handbook of mathematical functions with formulas, graphs, and mathematical tables. In: Applied

- Mathematics Series, vol. 55. National Bureau of Standards, Washington (fourth printing, December 1965).
- Andreas, E.L., Emanuel, K.A., 2001. Effects of sea spray on tropical cyclone intensity. *J. Atmos. Sci.* 58, 3741–3751.
- Brickman, D., Frank, K.T., 2000. Modelling the dispersal and mortality of Browns Bank egg and larval haddock (*Melanogrammus aeglefinus*). *Can. J. Fish. Aquat. Sci.* 57, 2519–2535.
- Chapron, B., Collard, F., Ardhuin, F., 2005. Direct measurements of ocean surface velocity from space: interpretation and validation. *J. Geophys. Res.* 110, C07008.
- Donelan, M.A., Pierson, W.J.P., 1987. Radar scattering and equilibrium ranges in wind-generated waves with application to scatterometry. *J. Geophys. Res.* 92, 4971–5029.
- Ekman, V.W., 1905. On the influence of the earth's rotation on ocean currents. *Arch. Math. Astron. Phys.* 2, 1–52.
- Emanuel, K.A., 1999. Thermodynamic control of hurricane intensity. *Nature* 401, 665–669.
- Farmer, D.M., D'Asaro, E.A., Trevorrow, M.V., Dairiki, G.T., 1995. Three-dimensional structure in a tidal convergence front. *Cont. Shelf Res.* 15, 1649–1673.
- Gemrich, J.R., Farmer, D.M., 2004. Near-surface turbulence in the presence of breaking waves. *J. Phys. Oceanogr.* 34, 1067–1086.
- Hasselmann, K., 1970. Wave-driven inertial oscillations. *Geophys. Fluid Dyn.* 1, 463–502.
- Hasselmann, S., Hasselmann, K., Komen, G.K., Janssen, P., Ewing, J.A., Cardone, V., 1988. The WAM model—a third generation ocean wave prediction model. *J. Phys. Oceanogr.* 18, 1775–1810.
- Huang, N.E., 1971. Derivation of Stokes drift for a deep-water random gravity wave field. *Deep-Sea Res.* 18, 255–259.
- Huang, N.E., 1979. On surface drift currents in the ocean. *J. Fluid Mech.* 91, 191–208.
- Jenkins, A.D., 1986. A theory for steady and variable wind and wave induced currents. *J. Phys. Oceanogr.* 16, 1370–1377.
- Jenkins, A.D., 1987a. A Lagrangian model for wind- and wave-induced near surface currents. *Coastal Eng.* 11, 513–526.
- Jenkins, A.D., 1987b. Wind and wave induced currents in a rotating sea with depth varying eddy viscosity. *J. Phys. Oceanogr.* 17, 938–951.
- Jenkins, A.D., 1989. The use of a wave prediction model for driving a near surface current model. *Dtsch. Hydrogr. Z.* 42, 134–149.
- Kelly, K.A., Dickinson, S., McPhaden, M., Johnson, G.C., 2001. Ocean currents evident in satellite wind data. *Geophys. Res. Lett.* 28, 2469–2472.
- Kenyon, K.E., 1969. Stokes drift for random gravity waves. *J. Geophys. Res.* 74, 6991–6994.
- Komen, G.J., Cavaleri, L., Donelan, M., Hasselmann, K., Hasselmann, S., Janssen, P.A.E.M., 1994. *Dynamics and Modelling of Ocean Waves*. Cambridge University Press, Cambridge.
- Leibovich, S., 1997a. Surface and near-surface motion of oil in the sea: Part I. Final Report to US Minerals Management Service, Contract 14-35-0001-30612, 136pp.
- Leibovich, S., 1997b. Surface and near-surface motion of oil in the sea: Part II. Final Report to US Minerals Management Service, Contract 14-35-0001-30612, 24pp.
- Lewis, D.M., Belcher, S.E., 2004. Time-dependent, coupled, Ekman boundary layer solutions incorporating Stokes drift. *Dyn. Atmos. Oceans* 37, 313–351.
- Longuet-Higgins, M.S., 1953. Mass transport in water waves. *Philos. Trans. R. Soc. London A* 245, 535–581.
- Longuet-Higgins, M.S., 1960. Mass transport in the boundary layer at a free oscillating surface. *J. Fluid Mech.* 8, 293–306.
- Madsen, O.S., 1977. A realistic model of the wind-induced Ekman boundary layer. *J. Phys. Oceanogr.* 7, 248–255.
- McWilliams, J.C., Sullivan, P.P., Moeng, C.H., 1997. Langmuir turbulence in the ocean. *J. Fluid Mech.* 334, 1–30.
- Mellor, G., Blumberg, A., 2004. Wave breaking and ocean surface layer thermal response. *J. Phys. Oceanogr.* 34, 693–698.
- Melsom, A., 1996. Effects of wave breaking on the surface drift. *J. Geophys. Res.* 101 (C5), 12071–12078.
- Morinta, I., Sugioka, S., Kojima, T., 1997. Real-time forecasting model of oil spill spreading. In: *Proceedings of the 1997 International Oil Spill Conference*, American Petroleum Institute, Washington, DC, pp. 559–566.
- Perrie, W., Tang, C., Hu, Y., DeTracy, B.M., 2003. The impact of waves on surface currents. *J. Phys. Oceanogr.* 33, 2126–2140.
- Pollard, R.T., 1970. Surface waves with rotation: an exact solution. *J. Geophys. Res.* 75, 5895–5898.
- Polton, J.A., Lewis, D.M., Belcher, S.E., 2005. The role of wave-induced Coriolis–Stokes forcing on the wind-driven mixed layer. *J. Phys. Oceanogr.* 35, 444–457.
- Price, J., Sundermeyer, M.A., 1999. Stratified Ekman layers. *J. Geophys. Res.* 104, 20467–20494.
- Quilfen, Y., Chapron, B., Vandemark, D., 2001. The ERS scatterometer wind measurement accuracy: evidence of seasonal and regional biases. *J. Atmos. Oceanic Technol.* 18 (10), 1684–1697.
- Raschle, N., Ardhuin, F., Terray, E.A., 2006. Drift and mixing under the ocean surface: a coherent one-dimensional description with application to unstratified conditions. *J. Geophys. Res.* 111, C03016.
- Raschle, N., 2007. Wave effects on the ocean circulation. Ph.D. Thesis, Université de Bretagne Occidentale <<http://tel.archives-ouvertes.fr/tel-00182250/en/>>.
- Reiss, C., Pantelev, G., Taggart, C., Sheng, J., de Young, B., 2000. Observations on larval fish transport and retention on the Scotian Shelf in relation to geostrophic circulation. *Fish. Oceanogr.* 9, 195–213.
- Saetra, Øyvind., Albretsen, Jon., 2007. Sea-state-dependent momentum fluxes for ocean modeling. *J. Phys. Oceanogr.* 37, 2714–2725.
- Santiago-Mandujano, F., Firing, E., 1990. Mixed-layer shear generated by wind stress in the central equatorial Pacific. *J. Phys. Oceanogr.* 20, 1576–1582.
- Tang, C.L., Gui, Q., 1996. A dynamical model for wind-driven ice motion: application to ice drift on the Labrador Shelf. *J. Geophys. Res.* 101, 28,343–28,364.
- Tang, C.L., McFarlane, N.A., D'Alessio, S.J.D., 2002. Boundary layer models for the ocean and atmosphere. In: *Perrie, W. (Ed.), Atmosphere–Ocean Interactions*. WIT Press, pp. 223–264.
- Tang, C.L., Perrie, W., Jenkins, A.D., DeTracy, B.M., Hu, Y., Toulany, B., 2007. Observation and modeling of surface currents on the Grand Banks: a study of the wave effects on surface currents. *J. Geophys. Res.* 112, C10025.
- Terray, E.A., Drennan, W.M., Donelan, M.A., 1999. The vertical structure of shear and dissipation in the ocean surface layer. In: *Banner, M.L. (Ed.), Proceedings of the Symposium on the Wind-driven Air–Sea Interface*. ADFA Document Production Centre, Canberra, Australia, pp. 239–245.
- Ursell, F., 1950. On the theoretical form of ocean swell on a rotating earth. *Mon. Not. R. Astron. Soc. (Geophys. Suppl.)* 6, 1–8.
- Weber, J.E., 1983. Steady wind- and wave-induced currents in the open ocean. *J. Phys. Oceanogr.* 13, 524–530.
- Weber, J.E., Melsom, A., 1993. Transient ocean currents induced by wind and growing waves. *J. Phys. Oceanogr.* 23, 193–206.
- Wu, J., 1982. Wind-stress coefficients over sea surface from breeze to hurricane. *J. Geophys. Res.* 87 (C12), 9704–9706.